# Deep Learning-Based Terahertz Phased Array System Beam Compensation Algorithm for Space Radiation Environments

Chensheng Ma[1], Yuanzhi He[2(✉)], and Rongbing Chen[2]

[1] Institute of Systems Engineering, Academy of Military Sciences, Beijing, China
chensheng_ams@163.com
[2] 32008 Troops of PLA, Beijing, China
he_yuanzhi@126.com, chenrb_dian@hotmail.com

**Abstract.** Inter-satellite terahertz (THz) communications, enabled by abundant spectrum and highly directional beams, are a key technology for future space information networks. However, the extremely narrow beamwidth of THz signals makes the link highly sensitive to beam misalignment. In practical spaceborne THz phased arrays, space radiation and inherent hardware imperfections jointly cause radiation pattern distortion and additional pointing errors, leading to severe degradation in link performance. Although traditional optimization methods, such as genetic algorithms and convex optimization, have been shown to be effective for beam compensation, they often suffer from local optima, high computational complexity, long convergence time, and limited adaptability. To address these challenges, we propose a deep learning-based beam compensation algorithm for radiation-affected THz phased array systems. We develop a health-aware Res-UNet (HA-Res-UNet) compensation network that leverages array-state feedback for dynamic beam correction. We introduce a multi-scale health-mask attention module that embeds element-health priors into feature aggregation to suppress failed elements and emphasize compensable regions. Simulation results demonstrate that the proposed method achieves approximately 90.4% pointing error reduction, improves the average pointing accuracy by about 10.4 times, and effectively mitigates radiation pattern distortions caused by failed array elements.

**Keywords:** terahertz, deep learning, beam compensation, space radiation environments.

## 1 Introduction

With the continuous evolution of the sixth-generation mobile communication systems (6G) [1] and non-terrestrial networks (NTNs) [2], communication infrastructures are progressively extending from terrestrial domains into space, enabling integrated space–air–ground ubiquitous connectivity. Among these, inter-satellite links (ISLs), particularly high-speed links within low Earth orbit (LEO) constellations, have emerged as a critical infrastructure for achieving global coverage, real-time data relay, and autonomous networking capabilities [3]. To meet the stringent requirements of future ISLs in terms of ultra-high data rates and ultra-low latency, the THz band, benefiting from its extremely large available bandwidth and potential spectral efficiency, is widely regarded as a promising candidate for inter-satellite communications [4]. However, compared with microwave frequencies, THz systems exhibit much higher directionality and significantly narrower beamwidths, rendering the communication links highly sensitive to antenna pointing accuracy. Even minor perturbations may result in noticeable beam misalignment and coherent gain loss, thereby leading to severe link performance degradation [5].

From an engineering perspective, spaceborne THz phased array systems are inevitably affected by various hardware non-idealities, such as local oscillator (LO) phase noise and channel mismatches. Meanwhile, the harsh space radiation environment may cause gradual degradation or even complete failure of array elements or RF channel components [6], resulting in a reduced effective aperture, sidelobe level increase, and radiation pattern distortion, as well as additional pointing errors [7]. These impairments pose significant challenges to conventional analytical compensation methods and iterative optimization strategies that rely on accurate system parameters. On the one hand, acquiring comprehensive and precise error model parameters in practical systems is costly and often infeasible. On the other hand, although optimization approaches such as genetic algorithms and convex optimization are theoretically applicable, they typically suffer from high computational complexity, limited real-time capability, and poor adaptability to evolving error distributions, such as the accumulation of failed elements over time. Therefore, it is both necessary and urgent to develop a compensation mechanism capable of rapidly reconfiguring the array in a near-optimal manner to maximize system performance.

In recent years, deep learning has been extensively applied in wireless communications and antenna array signal processing, becoming a powerful tool for addressing complex nonlinearities and strong uncertainties. Several studies have investigated hardware impairments in massive MIMO systems and employed deep learning techniques for beamforming design [8], [9]. Other works have applied deep learning to radiation pattern synthesis and optimization for phased array antennas [10], [11]. These advances indicate that incorporating deep learning into the compensation of THz phased array systems operating in radiation-affected space environments has great potential to achieve more robust beam recovery under complex conditions involving multi-source error coupling and element failures.

Motivated by the above considerations, this paper proposes a deep learning-based beam compensation algorithm for THz phased array systems operating in space radiation environments. The main contributions of the paper are summarized as follows:

- We establish an array-level analytical framework for characterizing pointing errors and radiation-pattern distortions in spaceborne THz phased array systems under coupled LO phase noise and radiation-induced element failures.
- We design a HA-Res-UNet with health-mask attention that injects element-health priors as structural biases, enabling fast and robust inference of deployable phase/amplitude control commands under non-uniform element failures.
- We validate the proposed method on a 216 GHz 8×8 planar array and demonstrate substantial pointing error reduction and pattern distortion mitigation.

# 2 THz Phased Array System Model

## 2.1 Ideal System

As shown in Fig. 1, we consider a THz phased array architecture suitable for satellite platforms [12]. In this system, multiple signal streams are generated at the digital baseband, mixed and upconverted to an intermediate frequency (IF) using a LO, and then individually processed by amplitude and phase control modules to impose per-channel amplitude/phase settings. The resulting signals are further delivered through multiple RF chains to drive the antenna array, forming a directive narrow-beam radiation.

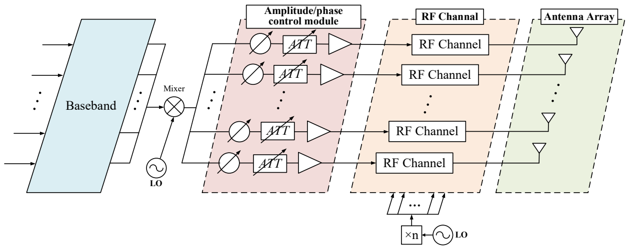


**Fig. 1.** Architecture of a Spaceborne THz Phased Array System.

## 2.2 Non-Ideal System

In principle, a THz phased array system can achieve accurate beam pointing through the amplitude and phase control modules. However, in practical implementations, beam pointing errors (BPEs) are still inevitable due to hardware non-idealities and the constraints imposed by the space environment. For the system shown in Fig. 1, we consider two dominant impairment sources: (i) phase noise introduced by the local oscillator (LO) chain and (ii) radiation-induced element failures in the space environment. These non-ideal factors degrade the intended amplitude/phase control by introducing element-wise amplitude and phase errors, which in turn lead to beam gain reduction, radiation-pattern distortion, and even beam pointing deviations.

# 3 Pointing Error Model

## 3.1 Array Theoretical Analysis

As shown in Fig. 2, we consider an $N_x \times N_y$ terahertz planar array placed on the $xoy$ coordinate plane. All array elements are assumed to be identical and uniformly spaced with half-wavelength inter-element spacing. We establish a Cartesian coordinate system with the upper-left array element as the origin. The observation point $p$ denotes the receiver location, and the corresponding elevation and azimuth angles are $\theta_0$ and $\varphi_0$, respectively. The radiation pattern of the $(m,n)$-th array element is denoted by $f_{mn}(\theta,\varphi)$. Let the excitation phase and amplitude of the $(m,n)$-th element be $\phi_{mn}$ and $A_{mn}$, respectively. The corresponding complex excitation can be expressed as in (1).

$$w_{mn} = A_{mn} e^{j\phi_{mn}} \tag{1}$$

When the following condition (2) holds, the far-field radiation pattern of the array antenna is steered toward point $p$.

$$\phi_{mn} = kd_x \sin\theta_0 \cos\varphi_0 + kd_y \sin\theta_0 \sin\varphi_0 \tag{2}$$

where $k = 2\pi / \lambda$ is the wavenumber. $d_x$ and $d_y$ represent the distances of $(m,n)$ -th element from the origin in the $x-$ and $y-$ directions, respectively. Accordingly, the far-field radiation pattern can be expressed as (3).

$$\begin{gathered} F(\theta,\varphi) = \sum_{m=0}^{N_x-1} \sum_{n=0}^{N_y-1} f_{mn}(\theta,\varphi) w_{mn} e^{-jku}, \\ (u = d_x \sin\theta \cos\varphi + d_y \sin\theta \sin\varphi) \end{gathered} \tag{3}$$

Assuming identical array elements and neglecting mutual coupling effects among elements, the array radiation pattern follows the pattern multiplication principle, i.e., the total radiation pattern can be expressed as the product of the element pattern $f_{mn}(\theta,\varphi)$ and the array factor $AF(\theta,\varphi)$. Thus, $AF(\theta,\varphi)$ can be rewritten as (4).

$$AF(\theta,\varphi) = \sum_{m=0}^{N_x-1} \sum_{n=0}^{N_y-1} w_{mn} e^{-jku} \tag{4}$$

From the above analysis, it can be observed that the element radiation pattern $f_{mn}(\theta,\varphi)$ depends only on the intrinsic properties of the antenna element, such as its shape, size, and type. In contrast, the array factor $AF(\theta,\varphi)$ is determined by the spatial arrangement of the array, element excitation conditions, and the number of elements, but is independent of the individual element radiation characteristics. Therefore, in beam-forming control, the array factor constitutes the primary focus of investigation.

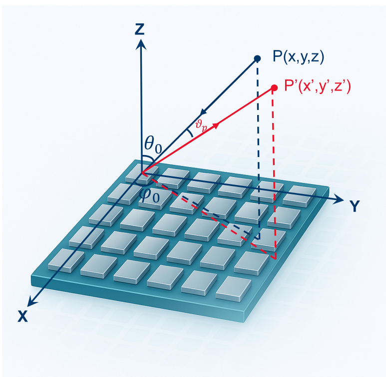


**Fig. 2.** Spatial geometry of the planar antenna array and the pointing direction.

### 3.2 Local Oscillator Phase Noise Model

For THz phased array systems, the LO signal is typically obtained by upconverting a low-frequency oscillator through a frequency-multiplication chain to the terahertz band. Due to the imperfections of practical oscillators, phase noise introduced by the oscillator and the multiplication chain inevitably exists. In addition, frequency multiplication effectively amplifies the phase noise generated by the oscillator. Therefore, the phase noise of the LO chain must be carefully modeled.

In this work, a multiple zero–pole phase noise power spectral density (PSD) model is adopted to characterize the phase fluctuation process [13]. The single-sideband phase noise PSD is expressed as in (5).

$$S_{\varphi}(f) = f_0 \frac{\prod_{i=1}^{3}\left(1+\left(f / f_{z,i}\right)^2\right)}{\prod_{i=1}^{3}\left(1+\left(f / f_{p,i}\right)^2\right)}, f \geq 0 \tag{5}$$

where $f_{z,i}$ and $f_{p,i}$ denote the frequencies of the zeros and poles, respectively. Considering that frequency multiplication leads to an effective increase in phase noise, a frequency-scaling factor $f_0$ is introduced and given by (6).

$$f_0 = 10\exp\left\{0.1\left[PSD_0 + 201og_{10}\left(f_{LO} / f_{LFO}\right)\right]\right\} \tag{6}$$

where $PSD_0$ represents the baseline phase noise PSD at the reference frequency, and $f_{LFO}$ denotes the frequency of the low-frequency oscillator.

### 3.3 Element Radiation Failure Model

In spaceborne THz phased array systems, high-energy particles may degrade or disable array elements and RF channel components, which degrades beam pointing performance. In this work, the element health state is characterized by a health factor to determine whether an element is functional or failed. We model the health status of each array element using a binary variable $h \in \{0,1\}$. A value of 1 corresponds to a fully functional element, and a value of 0 indicates total element failure induced by space radiation. Accordingly, the radiation pattern of a degraded array element can be modeled as the product of the ideal element pattern and the corresponding health factor, as in (7).

$$f_{mn,r}(\theta,\varphi) = f_{mn}(\theta,\varphi)\cdot h_{mn}(\theta,\varphi) \tag{7}$$

where $h_{mn}(\theta,\varphi)$ denotes the health factor of the $(m,n)$ -th element.

### 3.4 Pointing Error Angle Model

As shown in Fig. 2, under ideal conditions, the THz phased array system can form a far-field main lobe with maximum gain accurately pointing toward point $p$. However, when operating in complex space environments, the system is affected by the aforementioned impairment sources, causing the beam to deviate toward a shifted point $p'$.

By modeling the various impairment sources, we observe that these errors primarily affect the element radiation patterns and excitation phases. Therefore, all impairment effects are uniformly mapped to perturbations in the complex array excitations. The perturbed excitation of the $(m,n)$ -th array element can be expressed as in (8).

$$w_{mn,p}(\theta,\varphi) = h_{mn}(\theta,\varphi)\cdot e^{j\phi_{LO,mn}(\theta,\varphi)} \tag{8}$$

As a result, the far-field radiation pattern at point $p'$ can be written as (9).

$$F_p(\theta,\varphi) = F(\theta,\varphi)\cdot w_{mn,p}(\theta,\varphi) \tag{9}$$

The actual beam pointing direction $(\hat{\theta},\hat{\varphi})$ is determined by the location of the maximum radiation intensity, as in (10).

$$(\hat{\theta},\hat{\varphi}) = \arg\max_{\theta,\varphi}\left|F_p(\theta,\varphi)\right| \tag{10}$$

Accordingly, the pointing error angle is defined as in (11).

$$\vartheta_p = \sqrt{\left(\hat{\theta}-\theta\right)^2 + \left(\hat{\varphi}-\varphi\right)^2} \tag{11}$$

### 3.5 Error Analysis

Based on the established non-ideal system error models and the pointing error angle model, we investigate the performance of the THz phased array system under different impairment conditions. The desired beam direction is set to $(\theta_0,\varphi_0) = (40^\circ,20^\circ)$. Fig. 3 shows the polar patterns and the variation of the pointing error angle $\vartheta_p$. As shown in Fig. 3(a-b), the increase in the equivalent RMS phase error induced by LO phase noise is further amplified by the frequency-multiplication chain, resulting in a reduced main lobe peak and elevated sidelobes. Meanwhile, the main lobe peak drifts, causing $\vartheta_p$ to increase monotonically, which highlights the critical role of phase coherence in narrow-beam THz arrays. In Fig. 3(c-d), as the element failure ratio increases, the effective aperture shrinks, resulting in a continuous drop of the main lobe peak and an overall rise of the sidelobe floor; under severe failures, strong sidelobes compete with the main lobe, making $\vartheta_p$ increase and fluctuate more noticeably. Fig. 3(e-f) further shows that when both impairments coexist, the peak gap between the main lobe and sidelobes is reduced, so the maximum radiation direction is more easily dominated by sidelobes, yielding a larger and more unstable $\vartheta_p$.

Overall, although both impairment sources degrade array performance, their physical mechanisms differ. LO phase noise primarily drives coherent gain loss through phase inconsistency, whereas radiation-induced element failures cause aperture degradation and gain reduction, which can ultimately trigger pointing instability under extreme conditions.

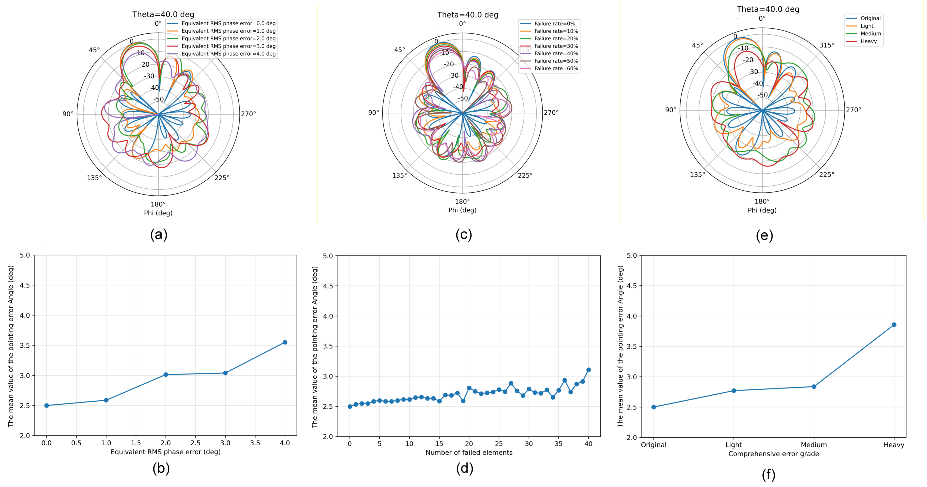


**Fig. 3.** Radiation-pattern degradation and pointing error under (a), (b) LO phase noise, (c), (d) element failures, and (e), (f) their coupling. Polar patterns are shown on the left, and mean pointing error angles are shown on the right.

# 4 Deep Learning-Based Health-Aware Compensation Architecture

In Section 3, mathematical models of various impairments in non-ideal THz phased array systems were established. Although approximate analytical solutions can, in principle, be derived from these models to compensate for the impairments, obtaining accurate information and precise model parameters for all error sources in practical systems is highly challenging. Therefore, in this section, we propose a deep-learning-based health-aware compensation architecture that enables real-time array compensation using neural networks. The proposed deep-learning-based health-aware compensation architecture consists of two stages: a ground-based supervised training stage and an on-orbit compensation stage.

## 4.1 Ground-based Supervised Training Stage

To effectively train the neural network, a labeled dataset is required to iteratively update the network parameters. However, due to the high cost, long cycle, and limited coverage of operating conditions associated with acquiring on-orbit THz payload data, it is difficult to obtain sufficient measurements from real spaceborne THz phased array systems. Therefore, the training data are generated via simulations based on the previously established error models.

Each training sample consists of network inputs and corresponding target values. In the considered scenario, the ideal pointing angles and the array health map are used as the input data, while the target values are the amplitude and phase control maps, i.e., the amplitude and phase control commands for each array element. Since the ideal pointing angle is a low-dimensional scalar, it is expanded into element-wise phase information using the relationship between the array pointing angle and the element phase difference given in (2).

Subsequently, phase noise perturbations are added to the element phases to form the array phase map. To avoid learning difficulties caused by $2\pi$ phase discontinuities, the input phase is encoded using trigonometric representations and expanded into two phase maps. The element amplitude map $A$ is assumed to be unity for all array elements. The array health map $H$ is generated based on the element health matrix $H \in \{0,1\}^{N_x \times N_y}$. Based on the array phase map and the health map, conventional optimization algorithms are employed to obtain the deployable amplitude control map $A_c$ and phase control map $\phi_c$, which serve as supervised labels. Accordingly, the labeled training dataset can be expressed as (12).

$$\Gamma = \left\{ \left( X^{(1)}, Y^{(1)} \right), \ldots, \left( X^{(N_t)}, Y^{(N_t)} \right) \right\} \tag{12}$$

where $N_t$ denotes the number of training samples. For the $i$-th sample, the input data and target values are given by (13) and (14).

$$X^{(i)} = \left( \cos\phi^{(i)}, \sin\phi^{(i)}, A^{(i)}, H^{(i)} \right) \tag{13}$$

$$Y^{(i)} = \left( \phi_c^{(i)}, A_c^{(i)} \right), i = 1, 2, \ldots, N_t \tag{14}$$

After obtaining the labeled training dataset $\Gamma$, we can apply it to train the proposed HA-Res-UNet. Given the input data $X^{(i)}$, the output of HA-Res-UNet can be expressed as (15).

$$\hat{Y}_\psi^{(i)} = g_\psi \left( X^{(i)} \right), \forall i \tag{15}$$

where $\psi$ denotes the set of network parameters and $g_\psi(\bullet)$ represents the mathematical model of HA-Res-UNet. To achieve effective compensation, the network parameters are iteratively updated by minimizing the discrepancy between the network output and the target values. This discrepancy is quantified using the empirical mean squared error (MSE). Accordingly, the loss function is defined as (16).

$$L_\Gamma(\psi) = \frac{1}{N_t} \sum_{i=1}^{N_t} \left\| Y^{(i)} - \hat{Y}_\psi^{(i)} \right\|^2 \tag{16}$$

Based on this loss function, the backpropagation algorithm is applied to update the network parameters by minimizing $\psi^* = \arg\min_\psi L_\Gamma(\psi)$. After training, the well-trained network with optimized parameters provides the compensation output for arbitrary input data.

### 4.2 On-Orbit Compensation Stage

The well-trained HA-Res-UNet is used for on-orbit compensation. Specifically, during on-orbit operation, the HA-Res-UNet model parameters $\psi^*$ obtained through ground-based offline training are fixed and deployed in the spaceborne processing unit. In each compensation cycle, the system constructs the network input according to the current array state, and outputs the array control commands through a single forward inference. These commands are then delivered to the phased array amplitude and phase control unit to complete rapid beam reconfiguration, thereby achieving real-time suppression of beam misalignment and radiation pattern distortion caused by local oscillator noise and element failures.

## 5 Network Architecture

To achieve beam compensation for THz phased array systems, we propose a health-aware Res-UNet (HA-Res-UNet), as shown in Fig. 4. It follows a multi-scale encoder-decoder backbone with downsampling/upsampling and skip connections to extract global features and recover fine details. To handle non-uniform defects caused by element failures, we introduce a health mask attention (HM-Attention) module at each scale, where the health map is used as a prior bias to suppress the influence of failed elements and emphasize compensable regions. This design improves the robustness of pointing correction and sidelobe control under high failure rates and phase-noise disturbances.

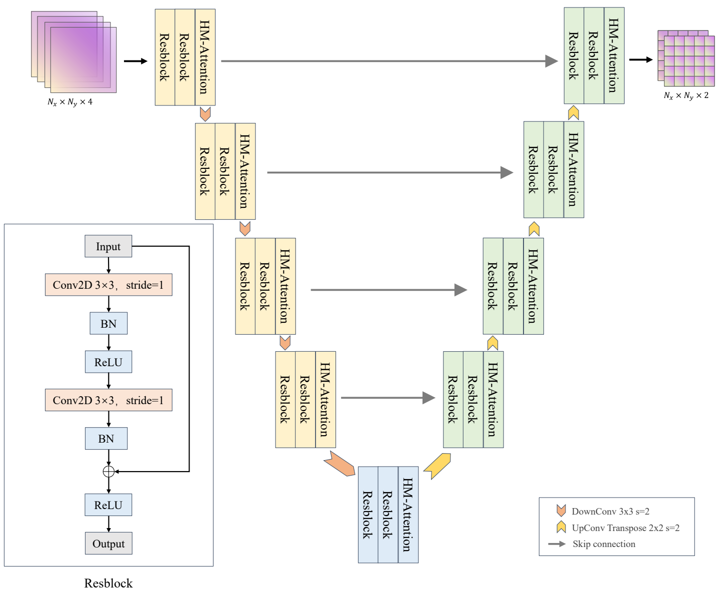


**Fig. 4.** Overview of the proposed HA-Res-UNet.

a) Backbone: Each residual block contains two 3×3 convolutions (stride 1) with BN, and ReLU after the first convolution; the input is added to the output for residual learning.

The encoder performs stride-2 convolutions to down sample and increase channels, while the decoder uses transposed convolutions to up sample; features are concatenated with same-scale encoder features and fused by residual blocks.

b) HM-Attention Module: HM-Attention is introduced at each scale to exploit element-health priors and enhance cross-element interactions. It performs spatial self-attention with two additive biases: a learned soft mask (modeling the diffusion of failure effects) and a health-derived hard bias (strongly penalizing failed elements).

# 6 Performance Evaluation

## 6.1 Simulation Setup

The simulation parameters are divided into two parts: system parameters and non-ideal system impairment parameters. For the system parameters, the array size $N_{\mathrm{x}} \times N_y$ is set to 8×8, with half-wavelength inter-element spacing. The carrier frequency is 216 GHz. A half-wave dipole element radiation pattern is adopted. For the non-ideal system impairment parameters, the low-frequency oscillator frequency is set to $f_{LFO} = 12GHz$, and the baseline phase noise power spectral density at the frequency offset is $PSD_0 = -79.4\mathrm{d}Bc/Hz$. The zero and pole frequency offsets are set to $\left\{f_{z,i}\right\} = \left\{1.8, 2.2, 40\right\} MHz$ and $\left\{f_{\mathrm{p},i}\right\} = \left\{0.1, 0.2, 8\right\} MHz$, respectively. The residual element ratio coefficients are set to $\left\{\kappa_{\varepsilon}\right\} = \left\{0.03, 0.05, 0.07, 0.09\right\}$.

To effectively train the proposed compensation network, supervised learning datasets are constructed based on the phase noise and element failure models presented in Section III. Specifically, we employ conventional optimization algorithms to compute the compensated array phase control map $\phi_{\mathrm{c}}$ and amplitude control map $A_{\mathrm{c}}$, which are then used as supervised labels. Finally, a total of 7804 valid samples are obtained and randomly divided into training, validation, and test sets with a ratio of 80%, 10%, and 10%, respectively. The partitioning is stratified according to element health regions to ensure consistency across data subsets. During network training, the Adam optimizer is employed, with an initial learning rate of $4\times10^{-4}$ and a weight decay of $1\times10^{-5}$. The batch size is set to 128, and the total number of training epochs is 200. To achieve adaptive learning rate adjustment, the learning rate is reduced by a factor of 0.9 when the validation loss does not decrease for four consecutive epochs. After training, the trained model is used for fast estimation of array control commands under different impairment conditions, enabling real-time compensation.

## 6.2 Compensation Performance

Preliminary results indicate that significant compensation performance can be achieved by training the network with fewer than 10,000 samples. As shown in Fig. 5, a sample is randomly selected from the test results. Under the target pointing direction $\left(\theta_0, \varphi_0\right) = \left(30^{\circ}, 35^{\circ}\right)$, the uncompensated far-field radiation pattern suffers from beam misalignment and sidelobe elevation due to the combined effects of LO phase noise and element failures, leading to reduced mainlobe gain and radiation-pattern distortion. After compensation, the main lobe is effectively restored toward the desired pointing direction, while sidelobe levels are suppressed. To further evaluate the effectiveness and computational efficiency of the proposed method, we compare HA-Res-UNet with the uncompensated array and the optimization-based label generation method. The results are summarized in Table 1. Without compensation, the mean pointing error angle reaches 0.7484°. The optimization-based label method achieves the lowest pointing error of 0.0587°, since it directly solves the compensation problem through iterative numerical optimization. However, this method requires approximately 1850 ms per sample, which makes it difficult to support real-time on-orbit beam reconfiguration. In contrast, the proposed HA-Res-UNet reduces the mean pointing error angle to 0.072°, corresponding to a 90.4% reduction compared with the uncompensated case. Although its pointing accuracy is slightly lower than that of the optimization-based method, HA-Res-UNet requires only 0.46 ms per sample through a single forward inference. These results indicate that HA-Res-UNet can approximate the optimization-based compensation results with substantially lower latency, suggesting its potential for real-time onboard deployment.

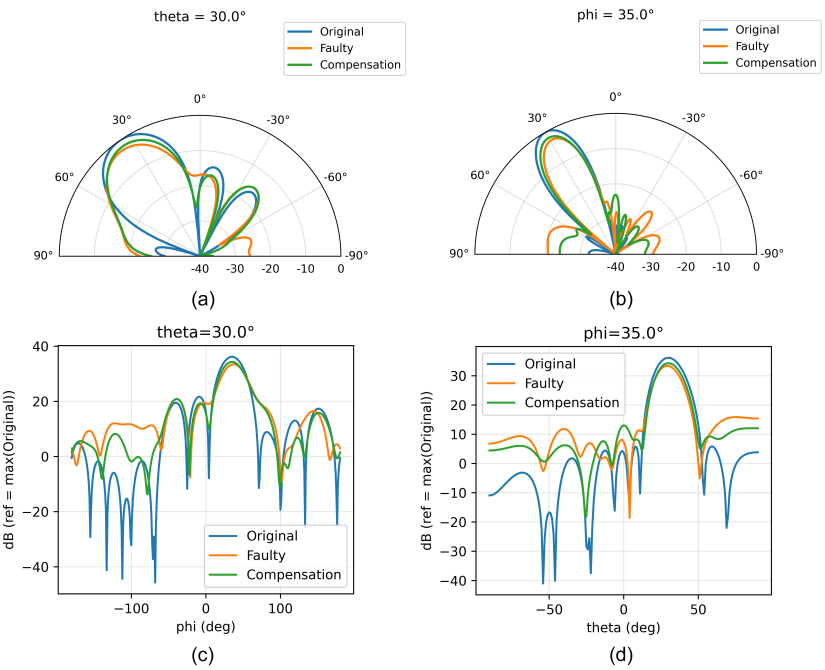


**Fig. 5.** Example far-field radiation patterns before and after HA-Res-UNet compensation: (a), (b) polar plots and (c), (d) plane patterns.

**Table 1.** Comparison with baseline beam compensation methods.

| | Mean pointing error angle | Runtime/sample |
|---|---|---|
| No compensation | 0.7484° | — |
| Optimization-based label method | 0.0587° | 1850 ms |
| HA-Res-UNet | 0.072° | 0.46 ms |

# 7 Conclusion

This paper focuses on spaceborne THz phased array systems operating in complex space radiation environments. To address beam misalignment and radiation pattern distortion caused by multiple non-ideal factors, including LO phase noise and radiation-induced element failures, a deep learning-based compensation method is proposed. By introducing a HA-Res-UNet compensation network, element health information is explicitly embedded into the multi-scale feature aggregation process, enabling robust beam correction under severe impairments. Simulation results demonstrate that the proposed method achieves approximately 90.4% pointing error reduction. The average pointing error decreases from 0.7484° (uncompensated) to 0.072°, and the pointing accuracy is improved by about 10.4 times, calculated as 0.7484/0.072≈10.4. The main lobe direction is effectively recovered, and radiation pattern distortions and sidelobe elevations are significantly mitigated, validating the effectiveness of the proposed approach.

# References


1. Saad W, Bennis M, Chen M: A vision of 6G wireless systems: applications, trends, technologies, and open research problems. IEEE Netw. **34**(3), 134–142 (2020).
2. Azari M.M, et al.: Evolution of non-terrestrial networks from 5G to 6G: a survey. IEEE Commun. Surveys Tuts. **24**(4), 2633–2672 (2022).
3. Nie S, Akyildiz I.F: Channel modeling and analysis of inter-small-satellite links in terahertz band space networks. IEEE Trans. Commun. **69**(12), 8585–8599 (2021).
4. He Y, Ma C: Research on frequency selection method for spatial terahertz communication under multiple constraints. In: 2022 IEEE 22nd International Conference on Communication Technology (ICCT), Nanjing, China, pp. 774–781 (2022).
5. He Y, Ma C: Analysis of the effect of antenna pointing error caused by satellite perturbation on space terahertz communication. Appl. Sci. **12**(21), 10772 (2022).
6. He Y, Ma C, Yin H: Measuring the radiation hardness of terahertz devices for space applications. Commun. Phys. **7**, 362 (2024).
7. Acharya O.P, Patnaik A: Antenna array failure correction [Antenna Applications Corner]. IEEE Antennas Propag. Mag. **59**(6), 106–115 (2017).
8. Che B, He Q, Chen Z, Quek T.Q.S: Deep learning based transceiver design for terahertz communication. IEEE Trans. Wireless Commun. **25**, 7235–7251 (2026).
9. Zhao, W., Han, C., Song, H.-J., Björnson, E.: DNN-Based Two-Stage Compensation Algorithm for THz Hybrid Beamforming With Imperfect Hardware. IEEE Trans. Wireless Commun. **25**, 1827–1841 (2026).
10. Tsai S.-M, Wu M.-T, Chen Y.-H, Yan H.-W, Chuang M.-L: Pattern compensation for faulty phased array antenna based on deep-learning technique. IEEE Open J. Antennas Propag. **6**, 414–421 (2025).
11. Merad L, Bendimerad F.T, Merah S: Neural networks for synthesis and optimization of antenna arrays. Radioengineering **16**(1), 23–30 (2007)
12. He, Y., Ma, C., Zhu, Z., An, J., Shen, W.: Terahertz Communication Payload Architecture for Space Information Networks: Challenges, Key Technologies, and Trends. IEEE Netw. **40**(1), 107–114 (2026).
13. 3GPP: Study on New Radio Access Technology: Radio Frequency (RF) and Co-existence Aspects, TR 38.803 V14.3.0 (Mar. 2022)